TRAIP drives replisome disassembly and mitotic DNA repair synthesis at sites of incomplete DNA replication

Remi Sonneville[1†], Rahul Bhowmick[2†], Saskia Hoffmann[3], Niels Mailand[3*], Ian D Hickson[2*], Karim Labib[1*]

[1]MRC Protein Phosphorylation and Ubiquitylation Unit, School of Life Sciences, University of Dundee, Dundee, United Kingdom; [2]Department of Cellular and Molecular Medicine, Center for Chromosome Stability, University of Copenhagen, Copenhagen, Denmark; [3]Novo Nordisk Foundation Center for Protein Research, Faculty of Health and Medical Sciences, University of Copenhagen, Copenhagen, Denmark

Abstract The faithful segregation of eukaryotic chromosomes in mitosis requires that the genome be duplicated completely prior to anaphase. However, cells with large genomes sometimes fail to complete replication during interphase and instead enter mitosis with regions of incompletely replicated DNA. These regions are processed in early mitosis via a process known as mitotic DNA repair synthesis (MiDAS), but little is known about how cells switch from conventional DNA replication to MiDAS. Using the early embryo of the nematode *Caenorhabditis elegans* as a model system, we show that the TRAIP ubiquitin ligase drives replisome disassembly in response to incomplete DNA replication, thereby providing access to replication forks for other factors. Moreover, TRAIP is essential for MiDAS in human cells, and is important in both systems to prevent mitotic segregation errors. Our data indicate that TRAIP is a master regulator of the processing of incomplete DNA replication during mitosis in metazoa.

DOI: https://doi.org/10.7554/eLife.48686.001

*For correspondence:
niels.mailand@cpr.ku.dk (NM);
iandh@sund.ku.dk (IDH);
kpmlabib@dundee.ac.uk (KL)

[†]These authors contributed equally to this work

Introduction

Chromosome duplication in eukaryotes is initiated from many origins of DNA replication on each chromosome, leading to the progression of DNA replication forks across the genome until fork convergence induces DNA replication termination. However, in species with genomes larger than about 100 Mb, it becomes increasingly likely that a small number of very late-replicating loci will not have completed DNA replication when cells enter mitosis (*Al Mamun et al., 2016*).

Metazoa have evolved pathways that quickly process sites of incomplete replication during mitosis, in order to facilitate the completion of chromosome segregation before cell division (*Bhowmick and Hickson, 2017*; *Moreno et al., 2016*). In human cells, factors such as the FANCD2 protein mark sites of unreplicated DNA, and then SLX4-dependent nucleolytic cleavage in mitosis promotes RAD52-dependent DNA repair synthesis (*Bhowmick et al., 2016*; *Minocherhomji et al., 2015*). Loci prone to such breakage and repair, particularly in response to DNA replication stress, include common fragile sites that are defined cytologically as breaks or gaps in metaphase chromosomes (*Glover et al., 2017*). Nevertheless, the mechanism by which mitotic processing initiates at such sites is not well understood. In particular, little is known about how conventional DNA replication forks are converted during mitosis into sites of DNA repair synthesis. One possibility is that the processing of sites of incomplete DNA replication begins with disassembly of the replisome, which otherwise protects the parental DNA at replication forks from attack by nucleases. The replisome is

assembled at origins of replication once per cell cycle, and is normally disassembled during DNA replication termination (*Dewar and Walter, 2017*; *Maric et al., 2014*; *Moreno et al., 2014*). Replisome disassembly is an active process, which is initiated by ubiquitylation of the CMG helicase via the ubiquitin ligase CUL-2^{LRR-1} (*Dewar et al., 2017*; *Sonneville et al., 2017*), leading to disassembly by the Cdc48 segregase and its essential co-factors Ufd1 and Npl4 (*Franz et al., 2011*; *Maric et al., 2017*).

Using the early embryo of *C. elegans* as a model system, we previously identified a mitotic pathway for CMG disassembly that also requires CDC-48_UFD-1_NPL-4, and is able to remove any post-termination replisomes that escape the normal disassembly process during S-phase (*Sonneville et al., 2017*). This mitotic pathway for replisome disassembly requires a ubiquitin ligase known as TRAIP (*Deng et al., 2019*; *Priego Moreno et al., 2019*), which is important for genome integrity in human cells (*Feng et al., 2016*; *Harley et al., 2016*; *Hoffmann et al., 2016*; *Soo Lee et al., 2016*) and is required to remove the replisome from converged DNA replication forks during the repair of inter-strand DNA crosslinks in extracts of *Xenopus laevis* eggs (*Wu et al., 2019*).

Very recently, it was shown that addition of mitotic cyclin-dependent kinase to *Xenopus* egg extracts induces TRAIP-dependent replisome disassembly (*Deng et al., 2019*; *Priego Moreno et al., 2019*), even when DNA replication is incomplete, and leads to fork breakage and DNA rearrangements (*Deng et al., 2019*). However, it has yet to be determined whether TRAIP is important in metazoan cells and tissues for replisome disassembly in response to incomplete DNA replication, and whether TRAIP is required for mitotic DNA repair synthesis at common fragile sites. Here, we address these issues, using an integrated approach that combines the advantages of the *C. elegans* early embryo and human cell lines as model systems.

Results and discussion

Replisome disassembly after incomplete DNA replication in the *C. elegans* early embryo requires the CDC-48_UFD-1_NPL-4 segregase

Monitoring replisome disassembly during mitosis is difficult in eukaryotic cells that have been exposed to DNA replication stress, since the S-phase checkpoint response usually blocks mitotic entry under such conditions. However, the *C. elegans* early embryo provides a useful model system in this regard, since the checkpoint response to replication stress is attenuated, such that mitotic entry is delayed but not blocked (*Brauchle et al., 2003*; *Encalada et al., 2000*). Moreover, the transparent nature of the embryo facilitates live cell imaging.

We previously established a live cell assay for replisome disassembly in the first cell cycles of the *C. elegans* embryo (*Sonneville et al., 2017*), based on monitoring the presence or absence of a GFP-tagged subunit of the CMG helicase on condensing chromatin (*Figure 1A*; chromatin is visualised via mCherry-tagged histone H2B). To assay for the presence of the replisome on mitotic chromatin after subjecting cells to DNA replication stress, we depleted the RPA-1 component of the RPA single-strand binding protein complex by RNAi (*Figure 1B*, *Figure 1—figure supplement 1A*). As shown previously (*Sonneville et al., 2015*), chromosome condensation during prophase of the first mitotic cell cycle was impaired after depletion of RPA-1 (*Figure 1C*, *Figure 1—figure supplement 1B*), reflecting mitotic entry in the presence of incomplete DNA replication. The chromatin subsequently aligned on the metaphase plate, but anaphase was impaired due to multiple chromatin bridges (*Figure 1C*, *Figure 1—figure supplement 1B*; compare *rpa-1* RNAi with control). Strikingly, components of the CMG helicase, such as the GINS subunits PSF-1 and SLD-5, and the CDC-45 protein, were not detected on the partially replicated chromatin during mitosis (*Figure 1C–D*, metaphase; *Figure 1—figure supplement 1C–D,F–H*). This reflected active disassembly of the CMG helicase by the CDC-48_UFD-1_NPL-4 segregase, since CMG components were retained on mitotic chromatin when NPL-4 and RPA-1 were depleted simultaneously (*Figure 1B–D*; *Figure 1—figure supplement 1A,C–D,F–H*; note that *npl-4* depletion also induced chromatin bridges, reflecting the multiple roles of CDC-48_UFD-1_NPL-4 during the cell cycle, including during mitosis). These data indicate that the replisome is disassembled before metaphase when DNA replication is perturbed in the *C. elegans* early embryo.

To confirm the link between replisome disassembly and incomplete DNA replication, we depleted ribonucleotide reductase via RNAi against *rnr-1* and thus depleted dNTPs. This produced a
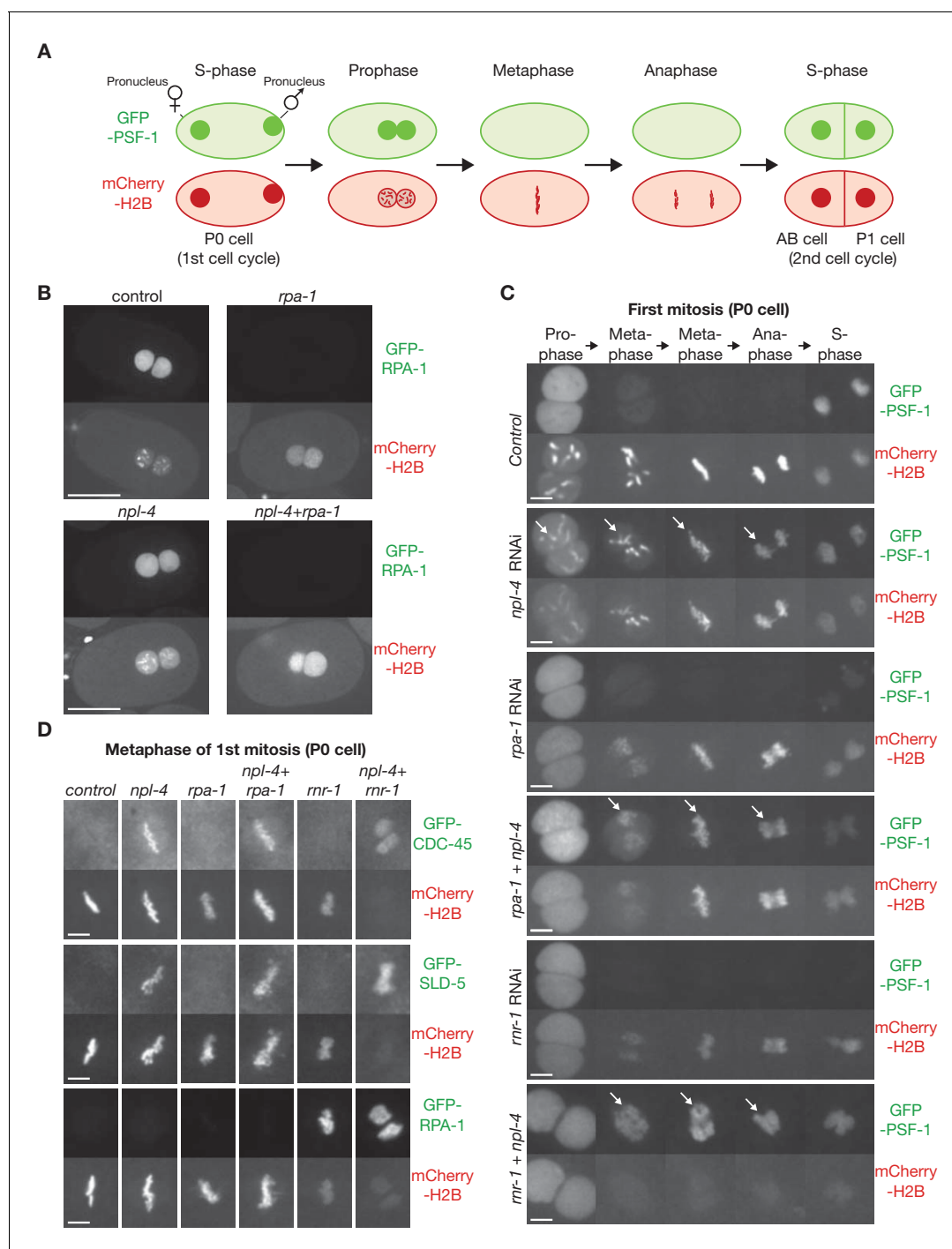
Figure 1. Incomplete DNA replication in *C. elegans* early embryos leads to unloading of the CMG helicase from chromatin by the CDC-48_UFD-1_NPL-4 segregase. (**A**) Illustration of the first cell cycle in the *C. elegans* early embryo. (**B**) Worms expressing GFP-RPA-1 and mCherry-Histone H2B were exposed to the indicated RNAi treatments (control = no RNAi). Images of whole embryos are shown, during prophase of the first embryonic cell cycle (two minutes before nuclear envelope breakdown), in order to illustrate the efficiency of RPA-1 depletion. (**C**) Worms expressing GFP-PSF-1 and mCherry-Histone H2B were exposed to the indicated RNAi treatments, before time-lapse imaging of the first mitosis in isolated embryos. The arrows indicate persistence of CMG on mitotic chromatin. (**D**) Worms expressing the indicated GFP-tagged replication proteins, together with mCherry-Histone H2B, were exposed to the same range of RNAi treatments as in (**C**). Examples are shown of the metaphase stage of the first embryonic mitosis. Scale bars = 20 μm in (**B**) and 5 μm in (**C and D**). Quantification of microscopy data is provided in *Figure 1—figure supplement 1*.

DOI: https://doi.org/10.7554/eLife.48686.002

The following figure supplements are available for figure 1:

Figure 1 continued on next page

Figure 1 continued

profound defect in DNA replication (*Sonneville et al., 2015*), as reflected by greatly impaired chromosome condensation during prophase (*Figure 1C*, *Figure 1—figure supplement 1B*; *Figure 1— figure supplement 2A–B* show that condensin II was not detected on mitotic chromatin after RNR-1 depletion). RPA accumulated on metaphase chromatin under such conditions (*Figure 1D*; *Figure 1— figure supplement 1F*), and chromosome segregation during anaphase was severely defective, thus blocking the subsequent reformation of the nuclear envelope (*Figure 1C*; 5 of 5 embryos examined behaved the same). CMG components were not detected on mitotic chromatin following *rnr-1* RNAi, mirroring the defect seen after depletion of RPA-1, and this was due to active disassembly of the replisome by CDC-48_UFD-1_NPL-4, since CMG components persisted on mitotic chromatin in embryos treated with *rnr-1 npl-4* double RNAi (*Figure 1C–D*, *Figure 1—figure supplement 1C–D, F–H*).

Interestingly, the mCherry-H2B signal was barely detectable throughout mitosis upon co-depletion of RNR-1 and NPL-4 (*Figure 1C–D*, *Figure 1—figure supplement 1E*), and this reflected the absence from mitotic chromatin of both condensin II and condensin I (*Figure 1—figure supplement 2*; note that condensin II normally associates with mitotic chromatin during prophase, whereas condensin I is loaded during metaphase). Most likely, the persistence of the CMG helicase at replication forks supported continued slow progression of the replisome throughout the genome, uncoupled from DNA synthesis, thereby unwinding the parental DNA duplex and displacing parental histones from unreplicated chromatin. In contrast, continued progression of the replisome in the presence of replication stress might be more limited following double RNAi to *rpa-1* and *npl-4*, such that a significant amount of unreplicated chromatin (marked by mCherry-H2B) persists across the genome. This issue is explored further below.

TRAIP is dispensable for proliferation in *C. elegans*, but preserves genome integrity in combination with CUL-2^{LRR-1}

To investigate whether the TRAIP ubiquitin ligase is required for mitotic replisome disassembly and the preservation of genome integrity in response to incomplete DNA replication in the *C. elegans* early embryo, we used CRISPR-Cas9 to delete the *trul-1* gene (*Figure 2—figure supplement 1*; TRUL-1 = TRAIP Ubiquitin Ligase 1). Interestingly, homozygous *trul-1Δ* worms are viable, in contrast to the lethality of previously reported deletions of TRAIP orthologues in the mouse and in *Drosophila* (*Merkle et al., 2009*; *Park et al., 2007*), probably reflecting the small number of cell divisions in the *C. elegans* life cycle and the relatively small size of the worm genome (around 100 Mb, compared to about 180 Mb in *Drosophila* and 1,500 Mb in mouse). Cell cycle progression appeared normal in homozygous *trul-1Δ* embryos (see below, *Figure 2—figure supplement 4*), but RNAi depletion of LRR-1 in *trul-1Δ* worms caused the persistence of the CMG helicase on mitotic chromatin (*Figure 2—figure supplement 2A–B*). A similar observation was made using *lrr-1 trul-1* double RNAi (*Deng et al., 2019*), confirming that TRUL-1 is required for the mitotic pathway that disassembles post-termination replisomes. Strikingly, LRR-1 depletion in *trul-1Δ* worms led to the appearance of anaphase DNA bridges in the early embryo (*Figure 2—figure supplement 2C*), indicating that the S-phase and mitotic pathways for replisome disassembly are jointly important for the preservation of genome integrity.

TRAIP is required for replisome disassembly in response to DNA replication stress

By exposing control and *trul-1Δ* worms to *rpa-1* RNAi, we observed that CMG persisted on mitotic chromatin when RPA-1 was depleted in the absence of TRAIP (*Figure 2A*, *Figure 2—figure supplement 3A*). In contrast, *rpa-1 lrr-1* double RNAi did not prevent replisome disassembly in wild type worms, and was equivalent to *rpa-1* single RNAi (*Figure 2A*, *Figure 2—figure supplement 3A*).
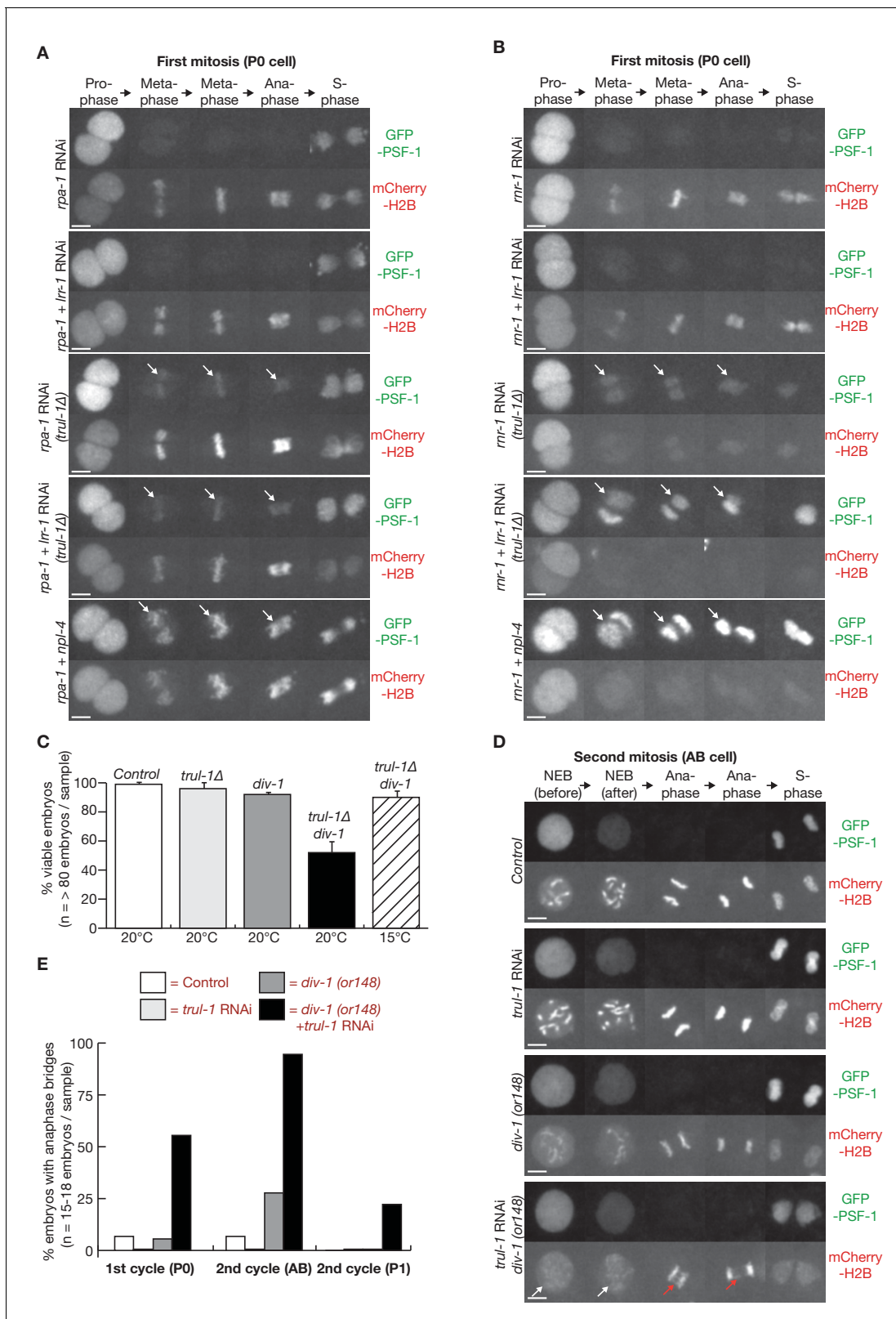
Figure 2. The TRUL-1 orthologue of human TRAIP is required for CMG unloading and genome integrity in response to incomplete DNA replication in *C. elegans* early embryos. (**A**) Videos of control and *trul-1Δ* embryos expressing GFP-PSF-1 and mCherry-Histone H2B, treated with RNAi to *rpa-1*, *lrr-1* and *npl-4* as indicated. Arrows indicate persistence of CMG on mitotic chromatin. (**B**) Videos of control and *trul-1Δ* embryos expressing GFP-PSF-1 and mCherry-Histone H2B, treated with the indicated RNAi treatments. Arrows indicate persistence of CMG on mitotic chromatin. (**C**) Embryonic viability

Figure 2 continued on next page

Figure 2 continued

was measured for the indicated strains, using worms grown at the temperatures shown. The data correspond to the mean and standard deviation from three independent experiments. (D) Videos of control and *div-1(or148)* temperature sensitive embryos expressing GFP-PSF-1 and mCherry-Histone H2B, treated with empty RNAi vector or RNAi to *trul-1* as indicated. In order to inactivate DIV-1, the worms were grown at the restrictive temperature of 25°C for 24 hr before imaging. The images correspond to division of the AB cell during the second embryonic cell cycle. White arrows indicate defective chromosome condensation during prophase, whereas red arrows denote chromatin bridges during anaphase. (E) Quantification of the percentage of cells with anaphase bridges in the first two embryonic cell cycles, for the experiment shown in (D). Scale bars in all microscopy images = 5 μm. Further quantification of microscopy data is provided in *Figure 2—figure supplement 3*.

The following figure supplements are available for figure 2:

Figure supplement 1. Deletion of the *C. elegans trul-1* gene by CRISPR-Cas9.

Figure supplement 2. TRUL-1 is required for disassembly of the CMG helicase during mitosis, and preserves genome integrity together with LRR-1.

Figure supplement 3. Quantification of *C. elegans* microscopy data in *Figure 2*.

Figure supplement 4. Timing of cell division for the first two embryonic cell cycles after inactivation of DIV-1 and TRUL-1.

Figure supplement 5. TRUL-1 is important for genome integrity and the successful completion of chromosome replication, when cells are exposed mild DNA replication stress, resulting from a diluted *rnr-1* RNAi.

These data indicated that replisome disassembly following RPA-1 depletion requires TRAIP, but is independent of the CUL-2^{LRR-1} pathway that acts when two converging replication forks encounter each other during DNA replication termination. Similarly, we observed that the CMG helicase accumulated on mitotic chromatin following *rnr-1* RNAi in *trul-1Δ* worms. However, this effect was enhanced in combination with *lrr-1* RNAi (*Figure 2B*, *Figure 2—figure supplement 3B*; compare *rnr-1* RNAi and *rnr-1 lrr-1* double RNAi in *trul-1Δ*). Moreover, mCherry-H2B on condensing chromatin was barely detectable throughout mitosis after *rnr-1 lrr-1* double RNAi in *trul-1Δ* worms, equivalent to the effect of *rnr-1 npl-4* double RNAi as discussed above (*Figure 2B*, *Figure 2—figure supplement 3B*). These findings are consistent with the notion that TRUL-1 normally mediates replisome disassembly following *rnr-1* RNAi, probably during mitosis (equivalent to TRAIP-dependent mitotic disassembly of post-termination replisomes). However, continued replisome progression in the absence of TRUL-1 allows some forks to converge, thereby leading to disassembly via the CUL-2^{LRR-1} pathway.

TRAIP preserves genome integrity and promotes survival in response to DNA replication stress

To investigate the physiological significance of the TRUL-1 pathway in response to incomplete DNA replication, we needed to use a milder form of DNA replication stress, since *rpa-1* and *rnr-1* RNAi both cause profound replication defects that prevent the successful completion of the first embryonic cell cycle. Initially, we used worms with a point mutation in the *div-1* gene, encoding the second-largest subunit of DNA polymerase alpha, since previous work showed that *div-1(or148ts)* worms are inviable at 25°C but can grow at lower temperatures (*Encalada et al., 2000*). Whereas the viability of *div-1* or *trul-1Δ* single mutants was close to that of the wild type control at the semi-permissive temperature of 20°C, the combination of *trul-1Δ* with *div-1* at 20°C produced synthetic lethality in around 50% of embryos. This synthetic lethality was suppressed by growth at the permissive temperature of 15°C (*Figure 2C*). These findings indicated that *C. elegans* TRAIP is important for worms to survive DNA replication stress, though TRUL-1 is dispensable in unperturbed cell cycles. It was not possible to compare *lrr-1* RNA with *trul-1Δ* in similar experiments, since depletion of LRR-1 is itself sufficient to produce DNA replication stress and lethality (*Merlet et al., 2010*).

To examine in greater detail how TRAIP contributes to the viability of *div-1* worms experiencing replication stress, we monitored the formation of anaphase chromatin bridges in the first two embryonic cell cycles of control or *div-1(or148ts)* worms grown at the restrictive temperature of 25°C, after treatment with *trul-1* RNAi or empty vector. As shown in *Figure 2D–E*, depletion of TRUL-1 led to

an accumulation of mitotic chromatin bridges in the *div-1* mutant (red arrows in *Figure 2D*), indicating that TRAIP is important for chromosome integrity in response to replication stress. In the second embryonic cell cycle, the effect was greatest (around 90% of embryos, n = 18) in the anterior AB cell (*Figure 1A*), which is known to have a weak S-phase checkpoint and thus is vulnerable to entering mitosis with persistent DNA replication stress (*Brauchle et al., 2003*). Conversely, chromatin bridges were observed less frequently in the posterior P1 cell. This cell has an enhanced checkpoint response (*Brauchle et al., 2003*), which greatly delays mitosis in response to replication stress (*Figure 2—figure supplement 4*), thereby providing more time to complete genome duplication. By carefully examining mitotic progression, we observed that chromosome condensation during prophase was partially defective in the AB cell but not the P1 cell of the *div-1(or148ts)* mutant, and this defect was exacerbated by depletion of TRUL-1 (*Figure 2D*, white arrows; *Figure 2—figure supplement 3C*). These data suggest that the AB cell of the *div-1(or148ts)* mutant enters mitosis before replication has been completed, and that TRUL-1 becomes important for the preservation of chromosome integrity under those conditions.

As an alternative way of inducing a low level of DNA replication stress, we fed worms on plates where bacteria expressing *rnr-1* RNAi were diluted with bacteria containing the empty RNAi vector (*Figure 2—figure supplement 5A*). Whereas the exposure of worms to 100% *rnr-1* RNAi caused a profound defect in condensation during prophase, and severe chromatin bridges during anaphase (*Figure 2—figure supplement 5B*, reproducing the phenotype shown in *Figure 1C*), mitosis progressed normally in most control embryos exposed to 10% *rnr-1* RNAi (*Figure 2—figure supplement 5C*). However, exposure of *trul-1Δ* worms to 10% *rnr-1* RNAi led to impaired condensation during prophase and chromatin bridges during anaphase (*Figure 2—figure supplement 5C–E*), thus reproducing the effect of combining *trul-1* RNAi with the *div-1*(or148ts) mutant (*Figure 2D*). Together with our earlier findings (*Deng et al., 2019*), these data indicated that TRUL-1 helps to preserve genome integrity in *C. elegans*, when cells enter mitosis in the presence of incomplete DNA replication.

TRAIP is required for FANCD2 focus formation and mitotic DNA repair synthesis at common fragile sites in human cells

To determine whether TRAIP has an evolutionarily conserved role in metazoa, and is required to process sites of incomplete DNA replication during mitosis, we monitored the appearance of mitotic DNA repair synthesis in human cells subjected to a low level of DNA replication stress. We used siRNA to deplete TRAIP in human U2OS cells (*Figure 3A*), and then treated cells with a low dose of the DNA polymerase inhibitor aphidicolin, before synchronisation in the G2-M phase of the cell cycle (*Figure 3B*). Subsequently, cells were released into mitosis in the presence of the nucleoside analogue EdU, and then harvested by mitotic shake off, before detection of FANCD2 foci and sites of EdU incorporation, as described previously (*Minocherhomji et al., 2015*). Strikingly, depletion of TRAIP with either of two different siRNAs suppressed the appearance of both FANCD2 and EdU foci (*Figure 3C–E*). Moreover, this defect was rescued by ectopic expression of an siRNA-resistant version of wild type TRAIP, but not by expression of mutant TRAIP that lacked a functional RING domain, which links the E3 ligase to its cognate E2 enzymes (*Figure 3F–H*). These data indicated that the ubiquitin ligase activity of TRAIP is required upstream of FANCD2 recruitment for mitotic DNA repair synthesis at sites of incomplete DNA replication in human cells. In contrast, depletion of LRR1 in human U2OS cells did not impair MiDAS (*Figure 3—figure supplement 1*).

Consistent with the *C. elegans* data described above, siRNA depletion of TRAIP in human cells led to an increase in anaphase DNA bridges, as well as ultrafine anaphase bridges coated with the PICH ATPase (*Figure 4A–B*). Previous studies have shown that the latter structures generally represent sites where incomplete DNA replication remains unresolved during mitosis (*Bhowmick and Hickson, 2017*). Moreover, cells in the subsequent G1-phase had an increased frequency of 53BP1 bodies (*Figure 4C*), which mark the persistence of sites of incomplete DNA replication from the previous cell cycle (*Lukas et al., 2011*; *Minocherhomji et al., 2015*; *Moreno et al., 2016*). Correspondingly, G1-phase cells also showed increased chromosomal instability in the form of micronuclei (*Figure 4D*). All of these phenotypes were rescued by expression of an siRNA-resistant form of TRAIP (*Figure 4*). These findings confirm that TRAIP is important for metazoan cells to process incomplete DNA replication during mitosis, thus preserving genome integrity.
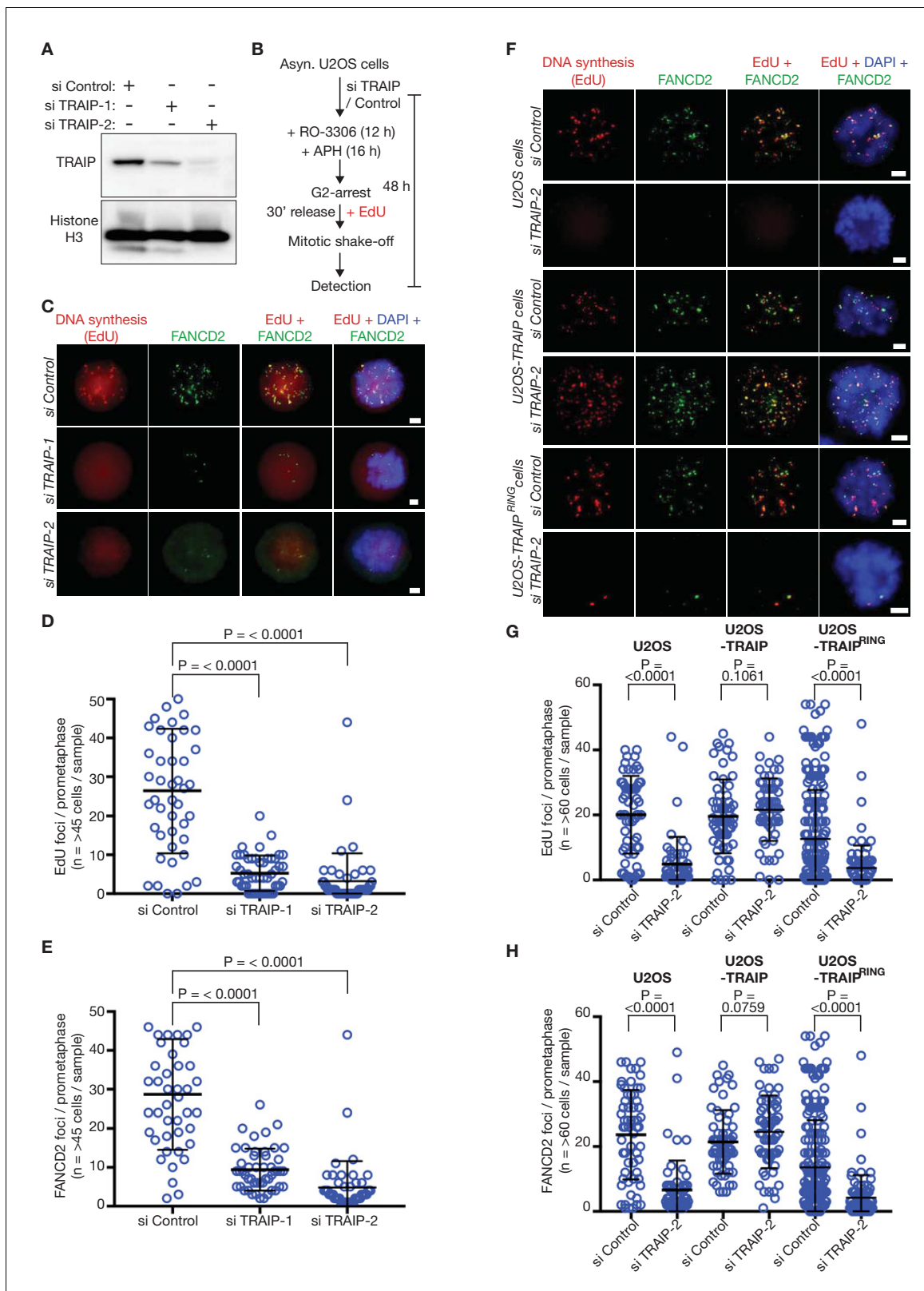
Figure 3. The TRAIP E3 ligase is required for mitotic DNA repair synthesis in response to DNA replication stress in human cells. (A) Immunoblots illustrating depletion of TRAIP by two specific siRNAs in human U2OS cells. (B) Experimental protocol: human U2OS cells were exposed to control siRNA or TRAIP-specific siRNA for 48 hr. During the last 16 hr of siRNA treatment, the cells were treated with the DNA polymerase inhibitor aphidicolin (APH), and the CDK1 inhibitor RO-3306 was then added for the final 12 hr of siRNA treatment to arrest the cells in G2-phase. Subsequently, the cells

Figure 3 continued on next page

Figure 3 continued

were released from G2-arrest in the absence of RO-3306 for 30 min in the presence of the nucleoside analogue EdU. Mitotic cells were harvested by mitotic shake-off and processed for markers of the mitotic pathway for DNA repair synthesis (foci of EdU incorporation that largely co-localise with foci of the FANCD2 protein). (C) Representative micrographs of 'prometaphase' mitotic cells treated as in (B). The scale bars correspond to 2 µm. (D) Quantification of the number of EdU foci per prometaphase cell. (E) Quantification of the number of FANCD2 foci per prometaphase cell. (F) U2OS control cells, U2OS cells expressing wild type TRAIP, and U2OS cells expressing a RING-mutant of TRAIP were treated as described above. Representative micrographs show EdU foci and FANCD2 foci in prometaphase cells. The scale bars correspond to 2 µm. (G) Quantification of the number of EdU foci per prometaphase cell. (H) Quantification of the number of FANCD2 foci per prometaphase cell. Note that ectopic expression of the TRAIP[RING] mutant causes a partial dominant negative phenotype (reduced frequency of EdU and FANCD2 foci, even with si Control), as seen previously (*Hoffmann et al., 2016*). For panels D-E and G-H, the broad horizontal lines represent the mean for the entire data set, and the shorter lines above and below denote the standard deviations. P-values were generated via a Mann-Whitney test.

DOI: https://doi.org/10.7554/eLife.48686.011

The following figure supplement is available for figure 3:

Figure supplement 1. Depletion of LRR1 does not block MiDAS in human U2-OS cells.

DOI: https://doi.org/10.7554/eLife.48686.012

Whereas S-phase was traditionally thought to end before the G2-phase of the cell cycle, it now appears that DNA replication in some parts of the genome can extend almost to the point of cell division. Such extremely late replicating regions of the genome include common fragile sites, but might also correspond to areas where two converging replication forks have both stalled in a region that lacks intervening dormant origins. Together with recent findings (*Deng et al., 2019*; *Priego Moreno et al., 2019*), our data indicate that TRAIP activity during mitosis promotes replisome disassembly at any remaining replication forks, thus exposing the parental DNA at the junction of the fork (we cannot exclude that TRAIP also has other important targets during mitosis, in addition to CMG). This leads to nucleolytic cleavage and mitotic DNA repair synthesis. In this way, mitotic TRAIP activity brings to an end the period during which conventional DNA replication is possible during the metazoan cell cycle. Although it remains to be demonstrated that TRAIP does indeed drive CMG helicase disassembly during mitosis in human cells, we have recently found that mouse TRAIP is required for mitotic CMG disassembly (Ryo Fujisawa, Fabrizio Villa and Karim Labib, unpublished data), indicating that the role of TRAIP is well conserved in diverse metazoan species.

As noted recently (*Deng et al., 2019*), if cleavage at each of two converging replication forks is specific to the leading strand template, which is normally encircled and thus protected by the CMG helicase, then one intact chromosome would rapidly be restored by gap filling, whereas repair of the other would require the joining of two broken ends. The latter would be associated with a small deletion and with sister chromatid exchange, thus matching the known features of common fragile sites in human cells (*Glover et al., 2017*). Our data indicate that TRAIP preserves viability when metazoan cells enter mitosis with incomplete replication, by promoting a programmed pathway of breakage and repair. This comes at the price of localised genome rearrangements, but avoids the far more damaging random breakage of loci during cell division in the presence of unreplicated DNA.

Materials and methods

Key resources table

Reagent type (species) or resource	Designation	Source or reference	Identifiers	Additional information
Strain, strain background (*Caenorhabditis elegans*)	GFP-PSF-1; mCherry-Histone H2B	*Sonneville et al., 2017* PMID: 28368371.	strain name: KAL3	*psf-1(lab1[gfp::TEV::S-tag::psf-1 + loxP unc-119(+) loxP]); ltIs 37[pie-1p::mCherry::his -58 + unc-119(+)]*
Strain, strain background (*Caenorhabditis elegans*)	GFP-CDC-45; mCherry-Histone H2B	*Sonneville et al., 2012* PMID: 22249291.	strain name: TG1754	*unc-119(ed3) III; gtIs65[pie-1p::gfp::cdc-45 + unc-119(+)]; ltIs37*

Continued on next page

Continued

Reagent type (species) or resource	Designation	Source or reference	Identifiers	Additional information
Strain, strain background (*Caenorhabditis elegans*)	GFP-SLD-5; mCherry-Histone H2B	*Sonneville et al., 2012* PMID: 22249291.	strain name: TG1756	*unc-119(ed3) III; gtIs65[pie-1p::gfp::sld-5 + unc-119(+)]; ltIs37*
Strain, strain background (*Caenorhabditis elegans*)	GFP-RPA-1; mCherry-Histone H2B	*Sonneville et al., 2012* PMID: 22249291.	strain name: TG2368	*unc-119(ed3) III; gtIs65[pie-1p::gfp::rpa-1 + unc-119(+)]; ltIs37*
Strain, strain background (*Caenorhabditis elegans*)	*div-1(or148)* allele	*Encalada et al., 2000* PMID: 11112326.	strain name: EU548	*div-1(or148[P352L]) III*
Strain, strain background (*Caenorhabditis elegans*)	GFP-CAPG-1; mCherry-Histone H2B	*Collette et al., 2011* PMID: 22025633.	strain name: EKM36	*unc-119(ed3) III; cldIs[pie-1p::gfp::capg-1 + unc-119(+)]; ltIs37*
Strain, strain background (*Caenorhabditis elegans*)	GFP-KLE-2; mCherry-Histone H2B	*Sonneville et al., 2015* PMID: 26166571.	strain name: TG3828	*unc-119(ed3) III; gtIs3828[pie-1p::gfp::kle-2 + unc-119(+)]; ltIs37*
Strain, strain background (*Caenorhabditis elegans*)	*div-1(or148)*; GFP-PSF-1; mCherry-Histone H2B	This study	strain name: KAL60	*div-1(or148) III; psf-1(lab1) II; ltIs37*
Strain, strain background (*Caenorhabditis elegans*)	*trul-1Δ*	This study	strain name: KAL90	*trul-1Δ (lab3 [3134 bp deletion])II*
Strain, strain background (*Caenorhabditis elegans*)	*trul-1Δ*; *div-1(or148)*	This study	strain name: KAL139	*div-1(or148) III; trul-1(lab3) II*
Strain, strain background (*Caenorhabditis elegans*)	*trul-1Δ*; GFP-PSF-1; mCherry-Histone H2B	This study	strain name: KAL92	*trul-1Δ (lab3) psf-1(lab1) II; ltIs37*
Cell line (*H. sapiens*, Female)	U-2 OS	ATCC	Cat# ATCC HTB-96; RRID:CVCL_0042	
Cell line (*H. sapiens*, Female)	U-2 OS expressing siRNA-resistant human TRAIP (wild type)	*Hoffmann et al., 2016* PMID: 26711499		Generated by group of Niels Mailand, by transfection of U-2 OS cells with plasmid expressing siRNA-resistant human TRAIP (wild type)
Cell line (*H. sapiens*, Female)	U-2 OS expressing siRNA-resistant human TRAIP (ΔRING - lacking residues 7–50)	*Hoffmann et al., 2016* PMID: 26711499		Generated by group of Niels Mailand, by transfection of U-2 OS cells with plasmid expressing siRNA-resistant human TRAIP (ΔRING - lacking residues 7–50)
Antibody	Sheep polyclonal, Ce TRUL-1	This study	C.e. TRUL-1 (70–291)_MRC PPU Reagents and Services: SA607	Raised against residues 70–291 of C.e. TRUL-1 (MRC PPU Reagents and Services); use at 1:1000 for immunoblotting.

Continued on next page

Continued

Reagent type (species) or resource	Designation	Source or reference	Identifiers	Additional information
Antibody	Sheep polyclonal, Ce MCM-2	*Sonneville et al., 2017* PMID: 28368371.	C.e. MCM-2 (1–222)_MRC PPU Reagents and Services:S750D	Raised against residues 1–222 of C.e. MCM-2 (MRC PPU Reagents and Services); use at 1:3000 for immunoblotting.
Antibody	Sheep polyclonal, Ce CDC-45	*Sonneville et al., 2017* PMID: 28368371.	C.e. CDC-45 (1-222)_MRC PPU Reagents and Services: S782D	Raised against residues 1–222 of C.e. CDC-45 (MRC PPU Reagents and Services); use at 1:500 for immunoblotting.
Antibody	Sheep polyclonal, TRAIP	*Hoffmann et al., 2016* PMID: 26711499	Anti-TRAIP (human)	Raised against full length human TRAIP (Niels Mailand's group); use at 1:250 for immunoblotting.
Antibody	Sheep polyclonal, LRR1	This paper	M.m. LRR1 (1–160)_MRC PPU Reagents and Services:SA279	Raised against residues 1–160 of M.m. LRR-1 (MRC PPU Reagents and Services); use at 1:250 for immunoblotting.
Antibody	Rabbit polyclonal, Anti-GAPDH	Sigma-Aldrich	Cat# PLA0125	Use at 1:1000 for immunoblotting.
Antibody	Rabbit polyclonal, Anti-Histone H3	Abcam	Cat# ab1791; RRID:AB-302613	Use at 1:2000 for immunoblotting.
Antibody	Rabbit polyclonal, FANCD2	Novus Biologicals	Cat# NB100-182; RRID:AB-10002867	Use at 1:400 for immunofluorescence.
Antibody	Mouse monoclonal, Anti-PICH, clone 142-26-3	Millipore	Cat# 04–1540; RRID:AB-10616795	Use at 1:50 for immunofluorescence.
Antibody	Mouse monoclonal, 53BP1 (6B3E10)	Santa Cruz Biotechnology	Cat# sc-517281	Use at 1:500 for immunofluorescence.
Antibody	Goat polyclonal, Anti-Mouse IgG (whole molecule)–peroxidase conjugated	Sigma Aldrich	Cat# A4416; RRID:AB_258167	Use at 1:2000 for immunoblotting.
Antibody	Goat polyclonal Anti-Rabbit IgG (whole molecule), F(ab')two fragment—Peroxidase conjugated	Sigma Aldrich	Cat# A6667; RRID: AB_258307	Use at 1:2000 for immunoblotting.
Antibody	Donkey polyclonal, Anti-Sheep IgG (whole molecule)–Peroxidase conjugated	Sigma Aldrich	Cat# A3415; RRID:AB_258076	Use at 1:2000 for immunoblotting.
Antibody	Goat polyclonal, anti-Rabbit IgG (H+L) Cross-Adsorbed Secondary Antibody, Alexa Fluor 488	Invitrogen	Cat# A-11008; RRID: AB_143165	Use at 1:1000 for immunofluorescence.

Continued

| Reagent type (species) or resource	Designation	Source or reference	Identifiers	Additional information
Antibody	Goat polyclonal, anti-Rabbit IgG (H+L) Cross-Adsorbed Secondary Antibody, Alexa Fluor 568	Invitrogen	Cat# A-11011; RRID: AB_143157	Use at 1:1000 for immunofluorescence.
Antibody	Goat polyclonal, anti-Mouse IgG (H+L) Highly Cross-Adsorbed Secondary Antibody, Alexa Fluor 488	Invitrogen	Cat# A-11029; RRID:AB_138404	Use at 1:1000 for immunofluorescence.
Antibody	Donkey polyclonal, anti-Mouse IgG (H+L) Highly Cross-Adsorbed Secondary Antibody, Alexa Fluor 568	Invitrogen	Cat# A-10037; RRID:AB_2534013	Use at 1:1000 for immunofluorescence.
Sequence-based reagent	oligo to genotype *trul-1Δ*: Primer a	This study		5'-ACACCATAGCGATTGTTTCCGG-3'
Sequence-based reagent	oligo to genotype *trul-1Δ*: Primer b	This study		5'-CCGGTGGTTTTTCAGCTTCTCC-3'
Sequence-based reagent	oligo to genotype *trul-1Δ*: Primer c	This study		5'-GATTCGTGTGGATTTCTGCGGT-3'
Sequence-based reagent	ON-TARGETplus *LRR1* siRNA	Dharmacon	Cat# LQ-016820–01	
Sequence-based reagent	*TRAIP* siRNA # 1 (5'-GAACCAUUAU CAAUAAGCU-3')	Sigma-Aldrich	Custom synthesised	*Hoffmann et al., 2016* PMID: 26711499
Commercial assay or kit	Click-iT EdU Alexa Fluor 594 Imaging Kit	ThermoFisher Scientific	Cat# C10339	
Chemical compound, drug	Aphidicolin	Sigma-Aldrich	Cat# A0781	
Chemical compound, drug	RO-3306	Millipore	Cat# 217699	
Software, algorithm	Image processing using ImageJ software	ImageJ software (National Institutes of Health)		
Software, algorithm	Prism data analysis software	Graphpad		
Software, algorithm	Image processing using Fiji software	ImageJ		
Other	Lipofectamine RNAimax	Life Technologies	Cat#13778075	

C. elegans maintenance

The *C. elegans* strains were maintained according to standard procedures (*Brenner, 1974*) and were grown on 'Nematode Growth Medium' (NGM: 3 g / L NaCl; 2.5 g / L peptone; 20 g / L agar; 5 mg / L cholesterol; 1 mM CaCl$_2$; 1 mM MgSO$_4$; 2.7 g / L KH$_2$PO$_4$; 0.89 g / L K$_2$HPO$_4$). The following worm strains were used: KAL3 *psf-1(lab1[gfp::TEV::S-tag::psf-1 + loxP unc-119(+) loxP]); ltIs37[pie-1p::mCherry::his-58 + unc-119(+)]* (*Sonneville et al., 2017*), TG1754 *unc-119(ed3) III; gtIs65[pie-1p::gfp::cdc-45 + unc-119(+)]; ltIs37* (*Sonneville et al., 2012*), TG1756 *unc-119(ed3) III; gtIs65[pie-1p::gfp::sld-5 + unc-119(+)]; ltIs37* (*Sonneville et al., 2012*), TG2368 *unc-119(ed3) III; gtIs65[pie-1p::gfp::rpa-*
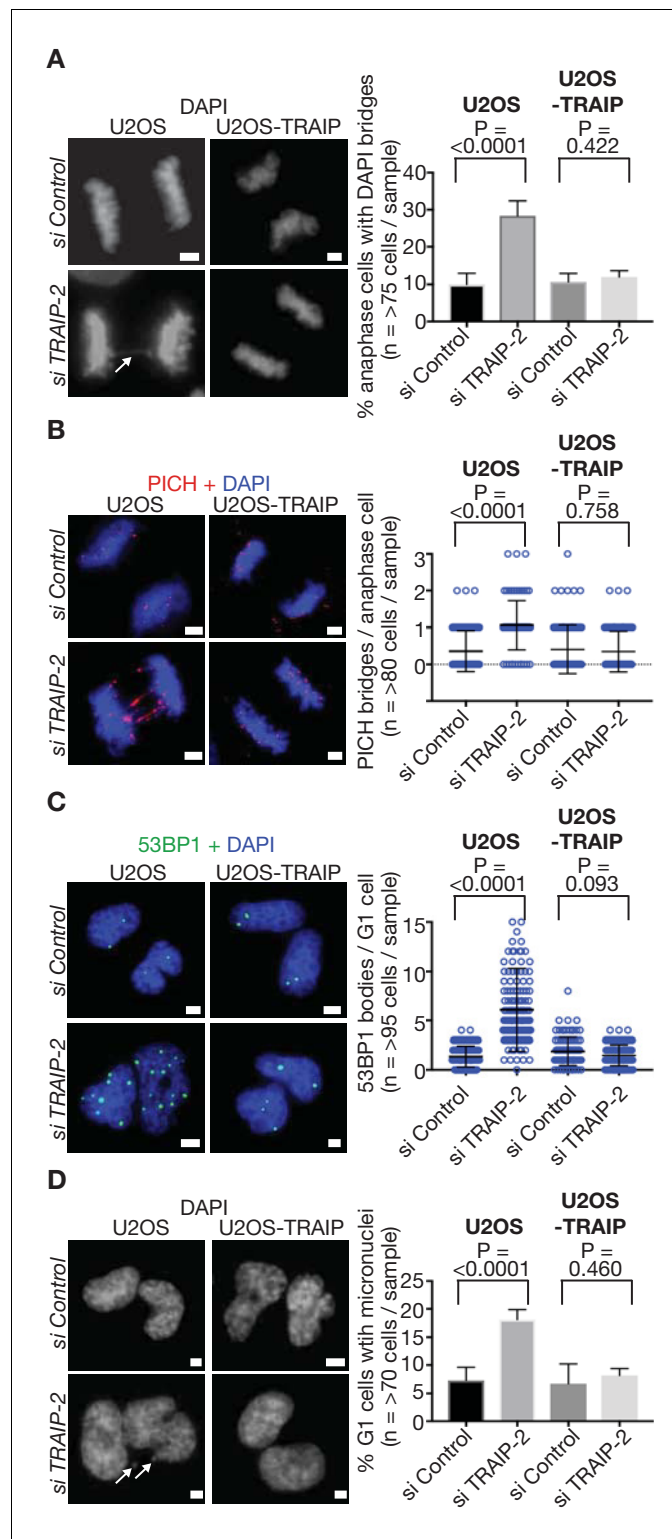
Figure 4. TRAIP is required to process sites of incomplete DNA replication and preserve genome integrity in response to DNA replication stress in human cells. (**A**) U2OS control cells and those expressing wild type TRAIP were treated as described in *Figure 3B*, except that cells were re-seeded onto plates for 15 min after mitotic shake-off, before detection of DAPI-positive DNA bridges in anaphase cells (white arrow denotes bridge - the data are quantified in the right-hand panel). (**B**) As per (**A**), except that ultra-fine DNA bridges were monitored by immunofluorescence detection of the PICH ATPase. Chromosomal DNA was detected by DAPI-staining. Note that

Figure 4 continued on next page

Figure 4 continued

the ultra-fine bridges are DAPI-negative. A quantification of the data is presented in the right-hand panel. (**C**) An analogous experiment to those above was performed, except that cells were re-seeded for 2.5 hr before detection of the 53BP1 protein by immunofluorescence in newly-born G1 cells. The number of 53BP1 bodies per G1-phase cell is quantified in the right-hand panel. (**D**) As per (**C**), except the number of micronuclei per G1-phase cell (indicated by white arrows) was determined by DAPI-staining. Statistics presented in this figure were calculated as described above for *Figure 3*. The scale bars correspond to 2 μm.

DOI: https://doi.org/10.7554/eLife.48686.013

1 + unc-119(+)]; ltIs37 (*Sonneville et al., 2012*), EU548 div-1(or148[P352L]) III (*Encalada et al., 2000*), EKM36 unc-119(ed3) III; cldIs[pie-1p::gfp::capg-1 + unc-119(+)]; ltIs37 (*Collette et al., 2011*), TG3828 unc-119(ed3) III; gtIs3828[pie-1p::gfp::kle-2 + unc-119(+)]; ltIs37 (*Sonneville et al., 2015*).

The following worm strains were made for this study: KAL60 div-1(or148) III; psf-1(lab1) II; ltIs37 was generated by crossing EU548 with KAL3. KAL90 trul-1Δ (lab3 [3134 bp deletion])II was generated using the CRISPR-CAS9 system (NemaMetrix) and trul-1Δ worms were out-crossed eight times with the N2 strain. KAL139 div-1(or148) III; trul-1(lab3) II was generated by crossing KAL90 with EU548. KAL92 trul-1Δ (lab3) psf-1(lab1) II; ltIs37 resulted from crossing KAL90 and KAL3.

C. elegans progeny viability assay

L4 worms (from a stock maintained at 15°C) were fed at 15°C for 72 hr, or at 20°C for 48 hr, and five adult worms were then transferred to a test plate for 150 min in order to lay embryos. The adult worms were then removed and the total number of embryos was counted (typically around 80 embryos). Subsequently, the number of embryos that developed into viable adults was determined and the embryonic viability was expressed as the ratio between the number of viable embryos and the total number of embryos.

RNA interference in C. elegans

RNAi was performed by feeding worms with RNAse III-deficient HT115 bacteria transformed with an L4440-derived plasmid that express double-stranded RNA (dsRNA) (*Timmons and Fire, 1998*). Bacterial culture (grown to OD600 = 1) was supplemented with 1 mM IPTG to express dsRNA. To titrate *rnr-1* RNAi, we mixed bacteria expressing *rnr-1* dsRNA with bacteria containing the empty vector. For example to obtain 10% *rnr-1* RNAi, 1 vol of culture of bacteria expressing *rnr-1* dsRNA was mixed with 9 volumes of control bacterial culture. Subsequently, 400 μl of bacteria were spread on a 6 cm RNAi plate (3 g / L NaCl, 20 g / L agarose, 5 mg / L cholesterol, 1 mM $CaCl_2$, 1 mM $MgSO_4$, 2.7 g / L KH_2PO_4, 0.89 g / L K_2HPO_4, 1 mM IPTG and 100 mg / L Ampicillin) and RNAi was induced overnight at room temperature.

The plasmids expressing dsRNA were made by cloning PCR products amplified from cDNA into the vector L4440 as described previously: *rnr-1* and *rpa-1* RNAi in *Sonneville et al. (2015)*; *npl-4* and *lrr-1* RNAi in *Sonneville et al. (2017)*; *trul-1* RNAi in *Deng et al. (2019)*. To target simultaneously *rnr-1* + *npl-4*, *rpa-1* + *npl-4*, *rnr-1* + *lrr-1* and *rpa-1* + *lrr-1*, DNA fragments corresponding to each gene were cloned contiguously into a single L4440 plasmid. The empty L4440 plasmid was used as a negative control throughout the RNAi experiments in this study.

Microscopy

Worms at the larval L4 stage were incubated on 6 cm RNAi feeding plates for 48 hr at 20°C. In the experiment using the *div1(or148ts)* mutant (*Figure 2D–E*), all worms were shifted to the restrictive temperature of 25°C for 24 hr, prior to imaging. For each experimental condition, five embryos were dissected from different worms in M9 medium (6 g / L Na_2HPO_4, 3 g / L KH_2PO_4, 5 g / L NaCl, 0.25 g / L $MgSO_4$) and mounted together on a 2% agarose pad. Embryos were then recorded simultaneously at 24°C, taking images every 10 s with 75% laser power and 200 milliseconds exposure time. Time lapse images were acquired using an Zeiss Cell Observer SD microscope with a Yokogawa CSU-X1 spinning disk, HAMAMATSU C13440 camera, fitted with a PECON incubator, using the ZEN blue software, and then processed with ImageJ software (National Institutes of Health) as previously described (*Sonneville et al., 2017*).

Quantification of signal intensity from *C. elegans* embryos

The GFP and mCherry signal intensity was evaluated during metaphase using ImageJ software (NIH). For each metaphase set of chromosomes, an area of fixed size was selected around the chromatin, and the integrated density was determined (the sum of the intensity of all pixels in the area). Subsequently, the data were adjusted for the background signal, by subtracting the integrated density of an area of equivalent size from the cytoplasm of the same embryo. The average signal intensity and standard deviation were then determined for five embryos per condition.

Genotyping worms

10 worms were lysed in 10 µl of buffer (1X PCR buffer, 1 mM MgCl2, 0.45% Tween-20) supplemented with 1.7 µg of Proteinase K at 60°C for 1 hr. The protease was inactivated at 95°C for 15 min and PCR was then performed using 0.5 µl lysed worms in a 25 µl reaction volume using Phusion polymerase (Biolabs). The following oligonucleotides were used to genotype the *trul-1Δ* and wild-type worms (as shown in *Figure 2—figure supplement 1*): Primer a 5'-ACACCATAGCGATTGTTTCCGG-3', Primer b 5'-CCGGTGGTTTTTCAGCTTCTCC-3' and Primer c 5'-GATTCGTGTGGATTTCTGCGGT-3'.

Extracts of worm embryos

Gravid adult worms from two 9 cm NGM plates were collected in M9 buffer and bleached with 10 ml of bleaching solution (for 100 ml: 36.5 ml H_2O, 45.5 ml 2 N NaOH and 18 ml ClNaO 4%) for about 8 min to release the embryos. The embryos were then washed twice with M9 buffer, suspended in 150 µl of M9 buffer and frozen on dry ice. Pellets were thawed and supplemented with 150 µl of 40% Trichloroacetic acid and 300 µl of glass beads. The cells were then broken by vortexing for one minute and the supernatant was collected. The beads were washed with 300 µl of 5% Trichloroacetic acid and the supernatant was added to the previous one. The extracts were then spun at 3000 rpm for 10 min and the pellet was re-suspended in 'high pH Laemmli buffer' (Laemmli buffer supplemented with 0.15 M Tris base).

Antibodies

The *C. elegans* TRUL-1 protein was detected with a sheep polyclonal antibody that was raised against amino acids 70–291 (MRC PPU reagents; SA607), whilst the anti-MCM-2 and anti-CDC-45 antibodies were described previously (*Sonneville et al., 2017*).

Primary antibodies specific for human PICH (1:50, 04–1540; Millipore), 53BP1 (1:500, sc-517281; Santa Cruz Biotechnology), FANCD2 (1:500, Novus Biologicals; NB100-182), TRAIP (1:250; Hoffmann et al – see Key Resources Table), GAPDH (1:1000, Sigma Aldrich; PLA0125), Histone H3 (1:2000, abcam; ab1791), were obtained from the indicated supplier. The corresponding secondary antibodies were: anti-mouse IgG (whole molecule peroxidase conjugate, 1:2,000, A4416; Sigma Aldrich), anti-rabbit IgG (whole molecule, F(ab')two fragment−peroxidase antibody produced in goat (1:2,000, A6667; Sigma Aldrich). Secondary antibodies used for immunofluorescence analysis of human cells were the Alexa Fluor 488 goat anti-rabbit IgG (1:1000, A-11008; Invitrogen), Alexa Fluor 568 goat anti-rabbit IgG (1:1000, A- A-11011; Invitrogen), Alexa Fluor 488 goat anti-mouse IgG (1:1000, A-11029; Invitrogen) and Alexa Fluor 568 donkey anti-mouse IgG (1:1000, A-10037; Invitrogen).

Human cell culture

U2OS osteosarcoma cells were maintained in Dulbecco's modified Eagle's medium (DMEM; Invitrogen, 11960), supplemented with 10% fetal bovine serum (FBS; Invitrogen, 10500) and 1% penicillin-streptomycin-glutamine (P-S-G; Invitrogen, 10378016). U2OS cells stably expressing either wildtype TRAIP (U2OS_TRAIP) or RING domain deleted TRAIP (U2OS_ΔRING TRAIP) were maintained similarly, except that the medium was supplemented with 5 µg / ml Blasticidin (Thermo Fisher Scientific, R21001) and 0.2 mg / ml Hygromycin B (Thermo Fisher Scientific, 10687010). All cells were maintained at 37°C in a humidified atmosphere containing 5% CO2. U2OS cells were obtained from the ATCC, and all cell lines were routinely tested for the absence of mycoplasma contamination (using MycoAlert; Lonza Group Ltd, LT07-318).

Human cell synchronisation

Asynchronously growing cells were treated with 7 μM RO-3306 (CDK1 inhibitor) for 12 hr to synchronise/arrest at the G2 phase of the cell cycle. The arrested cells were washed 3 times with warm DMEM medium and were then allowed to progress synchronously for 30 mins into prometaphase. The prometaphase cells were shaken off to be reseeded onto poly-lysine-coated slides, and were then either fixed or allowed to progress for 20 mins (anaphase) or 2.5 hr (G1 phase).

RNA interference treatment of human cells

Human TRAIP was depleted with either of two previously validated siRNAs (5'-GAACCAUUAUCAA UAAGCU-3'; 5'-CCGUGAUGAUAUUGAUCUCAA-3'). All siRNAs were custom synthesised by Sigma Aldrich with a 3'dTdT addition. In all transfection experiments, the 'Silencer-Select Control siRNA 2' (4390846, Ambion) was used as a negative control. For transient transfections, cells were seeded 12 hr prior to transfection in culture medium supplemented with FBS. The transfection was performed using lipofectamine RNAi Max reagent (Thermo Fisher Scientific, 13778030) according to the manufacturer's protocol.

EdU labelling and detection in human cells

EdU labelling and detection was performed as described previously (*Minocherhomji et al., 2015*). Click-IT chemistry was performed according to the manufacturer's instructions, but with a final concentration of 10X of the Click-IT EdU buffer additive (Life Technologies).

Immunofluorescence

Cells on glass cover slips or poly-lysine glass slides were fixed and permeabilised using cold PTEMF buffer (20 mM PIPES, pH 6.8, 10 mM EGTA, 0.2% Triton X-100, 1 mM $MgCl_2$ and 4% formaldehyde) for 20 mins at room temperature followed by blocking with PBSAT (0.5% Triton X in 3% BSA dissolved in PBS) for 20 mins at room temperature. Samples were then incubated with primary antibodies overnight at 4°C. Excess unbound primary antibody was removed by washing four times with PBSAT for 15 mins each. Samples were then incubated with secondary antibodies for 60 mins at room temperature, followed by four washes with PBSAT for 15 mins each. Air-dried slides or coverslips were mounted using VectaShield mounting medium with DAPI (Vector Laboratories). Images were captured using an Olympus BX63 microscope.

Statistics and reproducibility

The experiments were not randomised, no statistical method was used to predetermine sample size, and the investigators were not blinded to allocation during experiments and outcome assessment.

For *C. elegans* microscopy experiments, at least five embryos were analysed and seen to behave similarly, unless indicated otherwise. For *C. elegans* progeny viability assays, three biological replicates (independent experiments) were performed and the data represent the mean embryonic viability and the standard deviation for each condition. The PCR experiment in *Figure 2—figure supplement 1B* was performed 10 times, whereas the immunoblotting experiments in *Figure 2—figure supplement 1B* were performed 3 times, and those in *Figure 3A* were performed twice.

For work with human cells, at least 45–95 cells were examined per sample in the microscopy experiments (as indicated in *Figures 3–4*), and graphical and statistical analysis was carried out using 'Prism' software (GraphPad). At least three biological replicates were performed for each data set, which were then used to generate mean values and standard deviations. Statistical significance of these data was calculated using a Mann–Whitney U test (to minimise the effect of outliers in the data).

Acknowledgements

Additional information

Author contributions

Remi Sonneville, Conceptualization, Formal analysis, Validation, Investigation, Visualization, Methodology, Writing—original draft; Rahul Bhowmick, Formal analysis, Validation, Investigation, Visualization, Methodology, Writing—review and editing; Saskia Hoffmann, Resources, Formal analysis, Investigation, Methodology, Writing—review and editing; Niels Mailand, Resources, Formal analysis, Supervision, Funding acquisition, Investigation, Methodology, Writing—review and editing; Ian D Hickson, Resources, Formal analysis, Supervision, Funding acquisition, Validation, Investigation, Methodology, Writing—review and editing; Karim Labib, Conceptualization, Resources, Formal analysis, Supervision, Funding acquisition, Validation, Writing—original draft, Project administration

Author ORCIDs

Karim Labib (iD) https://orcid.org/0000-0001-8861-379X

Decision letter and Author response

Decision letter https://doi.org/10.7554/eLife.48686.016
Author response https://doi.org/10.7554/eLife.48686.017

Additional files

Supplementary files
• Transparent reporting form
DOI: https://doi.org/10.7554/eLife.48686.014

Data availability

All data generated or analysed during this study are included in the manuscript and supporting files.

References

Al Mamun M, Albergante L, Moreno A, Carrington JT, Blow JJ, Newman TJ. 2016. Inevitability and containment of replication errors for eukaryotic genome lengths spanning megabase to gigabase. *PNAS* **113**:E5765–E5774. DOI: https://doi.org/10.1073/pnas.1603241113, PMID: 27630194

Bhowmick R, Minocherhomji S, Hickson ID. 2016. RAD52 facilitates mitotic DNA synthesis following replication stress. *Molecular Cell* **64**:1117–1126. DOI: https://doi.org/10.1016/j.molcel.2016.10.037, PMID: 27984745

Bhowmick R, Hickson ID. 2017. The "enemies within": regions of the genome that are inherently difficult to replicate. *F1000Research* **6**:666. DOI: https://doi.org/10.12688/f1000research.11024.1, PMID: 28620461

Brauchle M, Baumer K, Gönczy P. 2003. Differential activation of the DNA replication checkpoint contributes to asynchrony of cell division in *C. elegans* embryos. *Current Biology* **13**:819–827. DOI: https://doi.org/10.1016/S0960-9822(03)00295-1, PMID: 12747829

Brenner S. 1974. The genetics of *Caenorhabditis elegans*. *Genetics* **77**:71–94. PMID: 4366476

Collette KS, Petty EL, Golenberg N, Bembenek JN, Csankovszki G. 2011. Different roles for Aurora B in condensin targeting during mitosis and meiosis. *Journal of Cell Science* **124**:3684–3694. DOI: https://doi.org/10.1242/jcs.088336, PMID: 22025633

Deng L, Wu RA, Sonneville R, Kochenova OV, Labib K, Pellman D, Walter JC. 2019. Mitotic CDK promotes replisome disassembly, fork breakage, and complex DNA rearrangements. *Molecular Cell* **73**:915–929. DOI: https://doi.org/10.1016/j.molcel.2018.12.021, PMID: 30849395

Dewar JM, Low E, Mann M, Räschle M, Walter JC. 2017. CRL2^Lrr1 promotes unloading of the vertebrate replisome from chromatin during replication termination. *Genes & Development* **31**:275–290. DOI: https://doi.org/10.1101/gad.291799.116, PMID: 28235849

Dewar JM, Walter JC. 2017. Mechanisms of DNA replication termination. *Nature Reviews Molecular Cell Biology* **18**:507–516. DOI: https://doi.org/10.1038/nrm.2017.42, PMID: 28537574

Encalada SE, Martin PR, Phillips JB, Lyczak R, Hamill DR, Swan KA, Bowerman B. 2000. DNA replication defects delay cell division and disrupt cell polarity in early *Caenorhabditis elegans* embryos. *Developmental Biology* **228**:225–238. DOI: https://doi.org/10.1006/dbio.2000.9965, PMID: 11112326

Feng W, Guo Y, Huang J, Deng Y, Zang J, Huen MS. 2016. TRAIP regulates replication fork recovery and progression via PCNA. *Cell Discovery* **2**:16016. DOI: https://doi.org/10.1038/celldisc.2016.16, PMID: 27462463

Franz A, Orth M, Pirson PA, Sonneville R, Blow JJ, Gartner A, Stemmann O, Hoppe T. 2011. CDC-48/p97 coordinates CDT-1 degradation with GINS chromatin dissociation to ensure faithful DNA replication. *Molecular Cell* **44**:85–96. DOI: https://doi.org/10.1016/j.molcel.2011.08.028, PMID: 21981920

Glover TW, Wilson TE, Arlt MF. 2017. Fragile sites in Cancer: more than meets the eye. *Nature Reviews Cancer* **17**:489–501. DOI: https://doi.org/10.1038/nrc.2017.52, PMID: 28740117

Harley ME, Murina O, Leitch A, Higgs MR, Bicknell LS, Yigit G, Blackford AN, Zlatanou A, Mackenzie KJ, Reddy K, Halachev M, McGlasson S, Reijns MAM, Fluteau A, Martin CA, Sabbioneda S, Elcioglu NH, Altmüller J, Thiele H, Greenhalgh L, et al. 2016. TRAIP promotes DNA damage response during genome replication and is mutated in primordial dwarfism. *Nature Genetics* **48**:36–43. DOI: https://doi.org/10.1038/ng.3451, PMID: 26595769

Hoffmann S, Smedegaard S, Nakamura K, Mortuza GB, Räschle M, Ibañez de Opakua A, Oka Y, Feng Y, Blanco FJ, Mann M, Montoya G, Groth A, Bekker-Jensen S, Mailand N. 2016. TRAIP is a PCNA-binding ubiquitin ligase that protects genome stability after replication stress. *The Journal of Cell Biology* **212**:63–75. DOI: https://doi.org/10.1083/jcb.201506071, PMID: 26711499

Lukas C, Savic V, Bekker-Jensen S, Doil C, Neumann B, Pedersen RS, Grøfte M, Chan KL, Hickson ID, Bartek J, Lukas J. 2011. 53bp1 nuclear bodies form around DNA lesions generated by mitotic transmission of chromosomes under replication stress. *Nature Cell Biology* **13**:243–253. DOI: https://doi.org/10.1038/ncb2201, PMID: 21317883

Maric M, Maculins T, De Piccoli G, Labib K. 2014. Cdc48 and a ubiquitin ligase drive disassembly of the CMG helicase at the end of DNA replication. *Science* **346**:1253596. DOI: https://doi.org/10.1126/science.1253596, PMID: 25342810

Maric M, Mukherjee P, Tatham MH, Hay R, Labib K. 2017. Ufd1-Npl4 recruit Cdc48 for disassembly of ubiquitylated CMG helicase at the end of chromosome replication. *Cell Reports* **18**:3033–3042. DOI: https://doi.org/10.1016/j.celrep.2017.03.020, PMID: 28355556

Merkle JA, Rickmyre JL, Garg A, Loggins EB, Jodoin JN, Lee E, Wu LP, Lee LA. 2009. No poles encodes a predicted E3 ubiquitin ligase required for early embryonic development of *Drosophila*. *Development* **136**:449–459. DOI: https://doi.org/10.1242/dev.027599, PMID: 19141674

Merlet J, Burger J, Tavernier N, Richaudeau B, Gomes J-E, Pintard L. 2010. The CRL2LRR-1 ubiquitin ligase regulates cell cycle progression during *C. elegans* development. *Development* **137**:3857–3866. DOI: https://doi.org/10.1242/dev.054866

Minocherhomji S, Ying S, Bjerregaard VA, Bursomanno S, Aleliunaite A, Wu W, Mankouri HW, Shen H, Liu Y, Hickson ID. 2015. Replication stress activates DNA repair synthesis in mitosis. *Nature* **528**:286–290. DOI: https://doi.org/10.1038/nature16139, PMID: 26633632

Moreno SP, Bailey R, Campion N, Herron S, Gambus A. 2014. Polyubiquitylation drives replisome disassembly at the termination of DNA replication. *Science* **346**:477–481. DOI: https://doi.org/10.1126/science.1253585, PMID: 25342805

Moreno A, Carrington JT, Albergante L, Al Mamun M, Haagensen EJ, Komseli ES, Gorgoulis VG, Newman TJ, Blow JJ. 2016. Unreplicated DNA remaining from unperturbed S phases passes through mitosis for resolution in daughter cells. *PNAS* **113**:E5757–E5764. DOI: https://doi.org/10.1073/pnas.1603252113, PMID: 27516545

Park ES, Choi S, Kim JM, Jeong Y, Choe J, Park CS, Choi Y, Rho J. 2007. Early embryonic lethality caused by targeted disruption of the TRAF-interacting protein (TRIP) gene. *Biochemical and Biophysical Research Communications* **363**:971–977. DOI: https://doi.org/10.1016/j.bbrc.2007.09.103, PMID: 17927961

Priego Moreno S, Jones RM, Poovathumkadavil D, Scaramuzza S, Gambus A. 2019. Mitotic replisome disassembly depends on TRAIP ubiquitin ligase activity. *Life Science Alliance* **2**:e201900390. DOI: https://doi.org/10.26508/lsa.201900390, PMID: 30979826

Sonneville R, Querenet M, Craig A, Gartner A, Blow JJ. 2012. The dynamics of replication licensing in live *Caenorhabditis elegans* embryos. *The Journal of Cell Biology* **196**:233–246. DOI: https://doi.org/10.1083/jcb.201110080, PMID: 22249291

Sonneville R, Craig G, Labib K, Gartner A, Blow JJ. 2015. Both chromosome decondensation and condensation are dependent on DNA replication in *C. elegans* embryos. *Cell Reports* **12**:405–417. DOI: https://doi.org/10.1016/j.celrep.2015.06.046, PMID: 26166571

Sonneville R, Moreno SP, Knebel A, Johnson C, Hastie CJ, Gartner A, Gambus A, Labib K. 2017. CUL-2LRR and UBXN-3 drive replisome disassembly during DNA replication termination and mitosis. *Nature Cell Biology* **19**: 468–479. DOI: https://doi.org/10.1038/ncb3500, PMID: 28368371

Soo Lee N, Jin Chung H, Kim H-J, Yun Lee S, Ji J-H, Seo Y, Hun Han S, Choi M, Yun M, Lee S-G, Myung K, Kim Y, Chul Kang H, Kim H. 2016. TRAIP/RNF206 is required for recruitment of RAP80 to sites of DNA damage. *Nature Communications* **7**:10463. DOI: https://doi.org/10.1038/ncomms10463

Timmons L, Fire A. 1998. Specific interference by ingested dsRNA. *Nature* **395**:854. DOI: https://doi.org/10.1038/27579, PMID: 9804418

Wu RA, Semlow DR, Kamimae-Lanning AN, Kochenova OV, Chistol G, Hodskinson MR, Amunugama R, Sparks JL, Wang M, Deng L, Mimoso CA, Low E, Patel KJ, Walter JC. 2019. TRAIP is a master regulator of DNA interstrand crosslink repair. *Nature* **567**:267–272. DOI: https://doi.org/10.1038/s41586-019-1002-0, PMID: 30842657